Cryogenic contact resistance and material conductivities in astronomic instrumentation: an experimental characterization.

Eduardo D. González-Carretero[1*], Haroldo Lorenzo-Hernández[1*], Antonio Zamora-Jiménez[1*] and Gualberto M. León-Cuesta[2]

[1] Mechanical Department, Instituto Astrofísica de Canarias, C. Vía Láctea SN, 38205, Spain.
[2]Physics Department, Universidad de La Laguna, C. Padre Herrera SN, 38200, Spain.

[*]Corresponding Authors:
Eduardo D. González Carretero: eduardo.glez.carretero@iac.es
Haroldo Lorenzo Hernández: haroldo.hernandez@iac.es
Antonio Zamora Jiménez: antonio.zamora.jimenez@iac.es

Abstract. Astronomic instrumentation requires working at cryogenic temperatures and a high stability. It is crucial to understand the properties of materials and contacts among components within the cryostat to be able to achieve the thermal goals in astronomical applications. To enhance instrument cold structure designs, there's a growing need to perform accurate Finite Element Method (FEM) analyses. Consequently, we conducted an experimental investigation to understand the properties of materials which we frequently employ in astronomical instrumentation at "Instituto de Astrofísica de Canarias" (IAC). The data will be used as an input to our FEM Models in order to minimize uncertainties. This paper presents an experimental study focused on cryogenic contact resistance and material conductivities vital for the advancement of astronomical instrumentation. The investigation is focused on the characterization of contact resistance and conductive properties at low temperatures, specifically for copper, stainless-steel and aluminium (for conduction), and nylon and PTFE (for insulation). Through in site experimentation, we explore the behaviour of materials under cryogenic conditions, providing valuable knowledge for optimizing the performance and reliability of astronomical devices and the way of designing contacts inside a cryostat.

1. Introduction

Astrophysics relies on highly precise instrumentation capable of operating under extreme, low-temperature conditions, necessitating materials with excellent thermal properties. High thermal conductivity materials like copper and gold are critical for efficient heat transfer and minimizing thermal resistance, particularly at contact interfaces[1]. Additionally, surface finishes enhance further thermal management by reducing the thermal gap in contacts[2]. These factors are essential for advancements in superconductivity, low-temperature physics, and space exploration, where stringent thermal control is paramount[3]. The study of thermal conductivities and conductances under cryogenic conditions is widely established within the scientific community due to its relevance in numerous scientific applications[4],[5],[6]. The IAC has long been at the forefront of developing astrophysical instrumentation. Its contributions span a wide array of projects from ground-based telescopes to space missions, supported by state-of-the-art facilities and specialized laboratories that enable research across visible, infrared, and microwave

wavelengths. Instrumentation developed at the IAC, such as TMS[7], MFI2[8], EMIR[9], LIRIS[10] and GRANCAIN[11] exemplifies the institute's commitment to scientific discovery and innovation. To advance further, its Department of Mechanics has initiated a new line of development focused on improving the reliability of thermal models. This involves detailed testing and characterization of materials to determine properties like specific heat capacity, thermal conductivity, thermal expansion, and thermal contact conductance under cryogenic conditions. Accurate experimental data are then used to feed FEM simulations, ensuring that these models align closely with real-world behaviour. The comprehensive material characterization will lead to more precise simulations and predictions, ultimately resulting in cryogenic systems that are optimized to meet the demanding conditions of cutting-edge scientific research.

2. Objectives

- Characterize Thermal Properties of Common Materials**:** This involves materials such as beryllium-copper, aluminium alloys, and stainless-steel.
- Validate FEM Models Against Experimental Data**.**

3. Experiment

The experiment was conducted at the IAC's headquarters in Tenerife, Canary Islands. The integration of the experimental setup took place in the clean room at the beginning of 2024. The cryostat used in this experiment was designed by the QUIJOTE consortium for installation in the TMS telescope at the Teide Observatory. The cryostat is engineered to cool the cold tip to 4K. It is a cylindrical cryostat made of AA6061-T6 aluminium alloy, featuring an inner volume of approximately 93 litres. The inner surface is mirror-polished to enhance its performance and cleanliness. The vacuum hardware includes the turbopump, a charcoal getter, electrical feedthroughs, gauges, and overpressure valves. The turbopump selected for the cryostat is the ATH 500 M from Pfeiffer. The cryogenic system, responsible for cooling the pixels and thermally isolated from the external environment, includes the Sumitomo RDK-415D cold head, the thermal links, the isolation structure and the shielding. Heat transmission by conduction is minimized using PTFE isolating legs. Moreover, the cooling of the instrument includes OFHC thermal links to minimize net heat exchange between the elements. The stages are shielded, and their surfaces are meticulously treated to achieve the lowest possible emissivity. This includes utilizing mirror-polished finishes or aluminized Mylar, which are highly effective in minimizing radiative heat transfer. Figure 1 shows the cryostat configuration and all its parts.

The test bars, including beryllium-copper, aluminium AA6061-T6, aluminium AA6082-T6, stainless-steel SS304, nylon and PFTE, were fabricated by the IAC's mechanical workshop, as depicted in the following Figure 1 in order to assess the thermal conductivity through the bars. The test tube was affixed to the cold finger of the second stage, and a ARCOL HS75 heater (electrical resistance) was installed in the upper part. Sensors were strategically placed along the test tube, with particular emphasis on two sensors positioned in the middle to capture temperature gradient measurements, with a distance of 20 centimetres between them. The sensors were securely attached using Apiezon®N grease designed for cryogenics, effectively sealing microscopic gaps between parts.

On the other hand, global nitrogen leakage and outgassing were evaluated with the evolution of the pressure inside the cryostat with the vacuum pump disconnected during different hours. The 64-hour vacuum vessel test yielded a nitrogen leakage rate of 7.99 x 10^{-5} mbar l/s (1.25 x

10^{-9} mbar l/s for helium), which is 1.5 times lower than the 124-hour measurement of 1.27 x 10^{-4} mbar l/s. Meanwhile, the resulting outgassing rates were 3.33 x 10^{-7} mbar l/s cm^2 for the former and 1.95 x 10^{-7} mbar l/s cm^2 for the latter. These values are reasonable and represent the characteristic performance of the TMS cryostat.

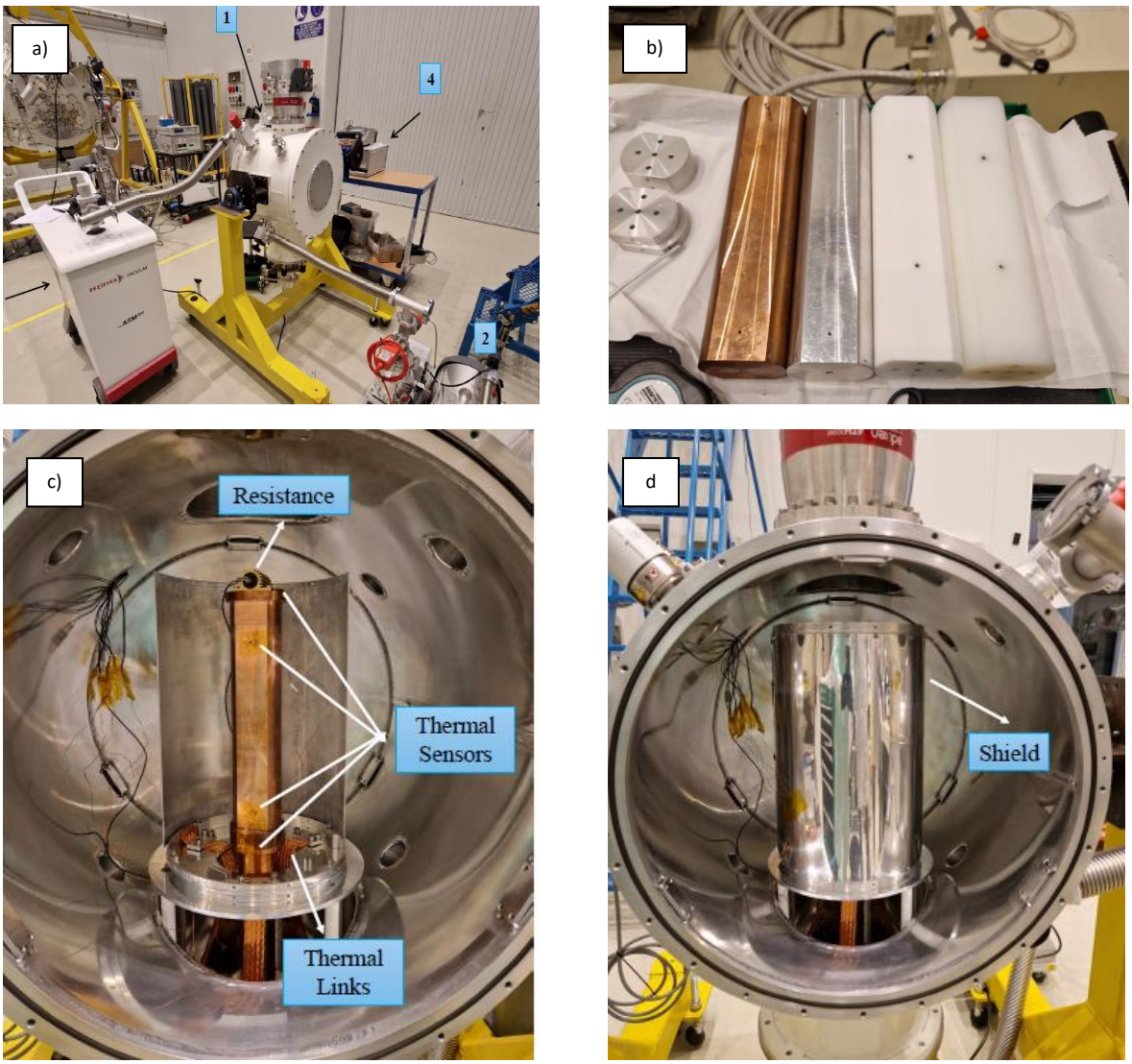

Figure 1. (a) Experiment setup for tests at the IAC's headquarters. (b) Test bars manufactured in different materials by the workshop of the IAC. (c) Setup for copper bar experiment. (d) Integration of the protective shield for the specimen.

4. Methodology

The methodology involves the experimental characterization of the thermal conductivity and conductance in materials commonly used in astronomical instrumentation (4-20K). The tests are based on monitoring the temperature sensors for an input power to the resistor, which will be assumed to be purely conductive, as radiation losses have been minimized.

Fourier's Law of Heat Conduction provides a mathematical framework for understanding how heat flows through a material. Meanwhile, thermal conductance is measured as a material's ability to transfer heat across the contact surface between two materials.

5. FEM Analysis

A thermal steady-state FEM model was built with the aim of estimating the cryocooler setpoint for different values of the resistor heat input. The vacuum chamber walls, both thermal shielding and the copper thermal straps were modelled by quadratic order shell elements. The isolators PTFE supports were modelled as low order beam elements. The sample piece, its holder and the resistor holder were modelled by quadratic order solid elements. To lighten the computational times, a half symmetry model was used; as it can be seen at Figure 2. All contacts were modelled as bonded with a perfect thermal contact conductance.

Regarding boundary conditions, three radiative heat transfer enclosures were defined: (1) between the vacuum chamber's inner surfaces and the outer surfaces of the 1st stage thermal shielding, (2) between the surfaces separating both thermal shielding, and (3) within the 2nd stage thermal shielding. A thermal emissivity of 0.1 was assigned to all surfaces involved. The resistor's heat input was modelled as a surface-applied natural boundary condition, while the vacuum chamber wall and cold tip temperatures for each stage were set as essential boundary conditions. Regarding the wall vessel temperature, it was fixed at 300 K (room temperature) and with respect to the cold-tips of the cryocooler, their nodal temperature was set to a value which comes from a multi-variable polynomial adjustment of the commercial capacity map, as seen in Figure 2. To set both temperature stages with a valid setpoint, the nodal heat of both cold-tips was used to feed an iterative process programmed in ANSYS Parametric Design Language (APDL). The polynomial adjustment on the range of interest of the capacity map shows a standard error of 0.34 K and 0.05 K for the 1st and 2nd stage temperatures, respectively. The thermal conductivity of the materials was modelled by NIST cryogenics database[12].

From the results of the simulation, it can be extracted that, below a resistor heat input from 0W to 10W, the radiative heat transferred to the sample piece can be neglected. Also, within this heat input range, the temperature at the spots where the sensors are placed was obtained (Figure 3). In the same picture, the temperature distribution for the case of a heat input of 5 W is showed. Both, the sample piece and the thermal shielding, show the expected longitudinal gradient due to the resistor heat input, similar to what was observed in empirical values.

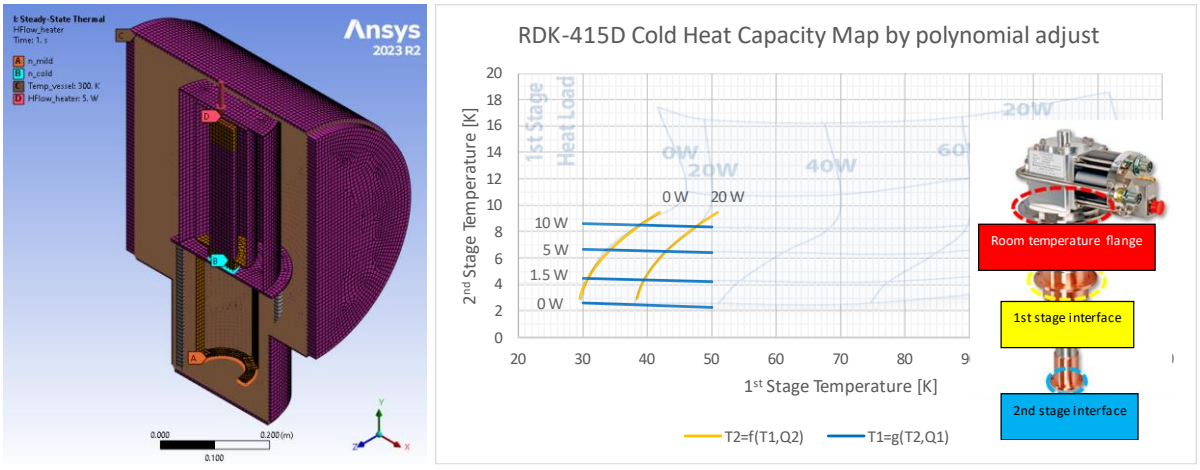

Figure 2. Left. FEM Model. A, B and C labels show the nodes where the essential boundary conditions were applied. D shows the surface where the heat flow which models the thermal resistor is placed. Right. RDK-415D cryocooler and its capacity map. Adjusted curves to a polynomial fit for the cold head capacity map.

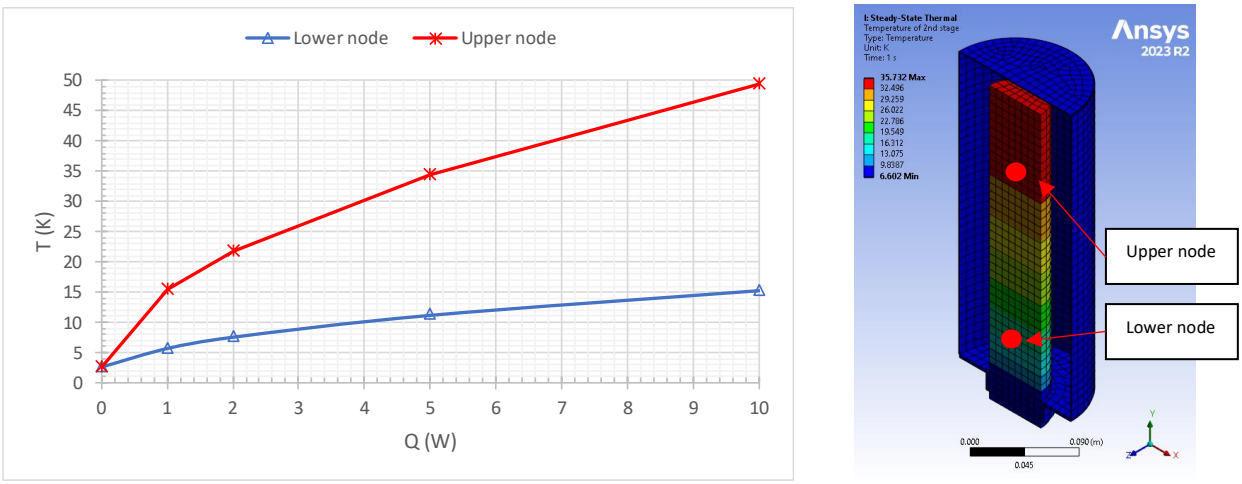

Figure 3. Left. Temperature value of the nodes of the FEM model located where the sensors were placed, as function of the resistor heat input. Right. Temperature distribution in the test bar for a 5 W inlet heat.

6. Results

To accurately characterize the thermal parameters of commonly used materials at IAC, a series of experiments regarding AA test bars were conducted under steady-state conditions as outlined in sections 4 and 5. This approach allowed us to correlate our setup with established literature data and to verify our experimental procedures that establish the parameters of the materials to be obtained and that are subsequently used in the FEM modelling of our instruments, specifically in the line of development of instruments in the microwave spectral range.

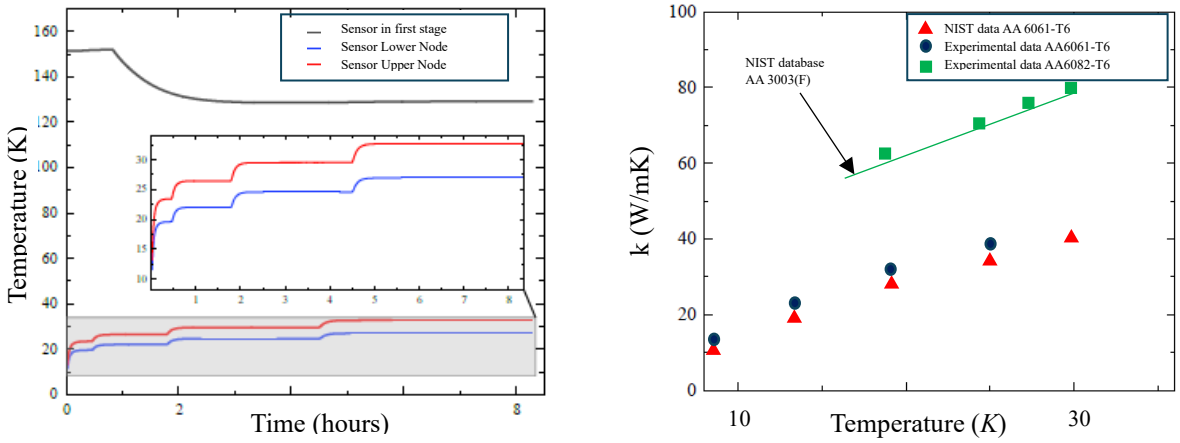

Figure 4. Left. Transient temperatures recorded for the AA6061-T6 bar as the resistor's inlet power was sequentially increased. The image displays temperature data from sensors positioned at both ends of the test bar for various inlet power levels (0.45W, 1.8W, 4.0W, 5.4W). Right. Thermal conductivity values obtained for AA6061-T6 and AA6082-T6, compared with reference values from the NIST database.

Figure 4 illustrates the temperature evolution as the resistor's input power increases. Additionally, by measuring the temperatures at both ends of the specimens, it is possible to calculate the thermal conductivity of the material at various cryogenic temperatures. For the AA6061-T6 alloy, the errors obtained were below 11%, whereas a significant discrepancy was observed for the AA6082-T6 alloy. While AA6061 and AA6082 are assumed to have similar

mechanical properties, their thermal properties differ notably at cryogenic temperatures. In fact, the thermal conductivity of AA6082 is approximately double that of AA6061 for temperatures between 0 and 50 K. As noted in the predictive study by Woodcraft A.[6] on the thermal properties of aluminium based on its RRR, the AA6082 alloy exhibits similarities to the AA3003 alloy. When making this comparison, the errors between the two materials were also on the order of 11%. These errors primarily stem from measurement inaccuracies of the sensors and residual heat losses inherent to the experimental setup.

8. Conclusions

Based on the results obtained in this manuscript, it can be concluded that precise results have been achieved for the conductivity of AA6061-T6 and AA6082-T6 aluminium in the specified temperature range. This is primarily due to the optimization of the sensor configuration and calibration, as well as the introduction of a corrective parameter in the incident heat power of the control volume, which minimizes the uncertainty in the conductive power through the sample. It can be inferred that the values obtained are very close to those found in the literature. Therefore, unless surface temperature precision at the mK level is required, the use of reference curves from the literature does not have a significant impact on the final results of the model. Prototypes made of beryllium-copper, and SS304 exhibited similar effects, although their study still needs to be thoroughly investigated. Contributions such as residual heat losses, emissivity of materials and thermal contacts can cause errors in the model exceeding 50%, having a much greater impact in the final results than the material's conductivity which are specified in the bibliography.

References

[1] R. C. Dhuley, “Pressed copper and gold-plated copper contacts at low temperatures – A review of thermal contact resistance,” *Cryogenics (Guildf)*, vol. 101, pp. 111–124, Jul. 2019, doi: 10.1016/J.CRYOGENICS.2019.06.008.

[2] R. S. Prasher and P. E. Phelan, “Microscopic and macroscopic thermal contact resistances of pressed mechanical contacts,” *J Appl Phys*, vol. 100, no. 6, Sep. 2006, doi: 10.1063/1.2353704.

[3] X. Pan, X. Cui, S. Liu, Z. Jiang, Y. Wu, and Z. Chen, “Research Progress of Thermal Contact Resistance,” *J Low Temp Phys*, vol. 201, no. 3–4, pp. 213–253, Nov. 2020, doi: 10.1007/s10909-020-02497-0.

[4] S. Sunil Kumar and K. Ramamurthi, “Thermal contact conductance of pressed contacts at low temperatures,” *Cryogenics (Guildf)*, vol. 44, no. 10, pp. 727–734, Oct. 2004, doi: 10.1016/j.cryogenics.2004.04.004.

[5] P. G. Siddappa and A. Tariq, “Contact area and thermal conductance estimation based on the actual surface roughness measurement,” *Tribol Int*, vol. 148, Aug. 2020, doi: 10.1016/j.triboint.2020.106358.

[6] A. L. Woodcraft, “Predicting the thermal conductivity of aluminium alloys in the cryogenic to room temperature range.” [Online]. Available: http://www.sciencedirect.com/science/journal/00112275

[7] P. Alonso-Arias *et al.*, “New technologies for the Tenerife Microwave Spectrometer and current status,” SPIE-Intl Soc Optical Eng, Dec. 2020, p. 63. doi: 10.1117/12.2561353.

[8] R. J. Hoyland *et al.*, “The new multi-frequency instrument (MFI2) for the QUIJOTE facility in Tenerife,” SPIE-Intl Soc Optical Eng, Jul. 2022, p. 185. doi: 10.1117/12.2640826.

[9] S. Barrera *et al.*, “EMIR optomechanics,” in *Astronomical Structures and Mechanisms Technology*, SPIE, Sep. 2004, p. 611. doi: 10.1117/12.550463.

[10] E. Hernandez *et al.*, “Mechanics of LIRIS (long-slit intermediate-resolution infrared spectrograph) at first commissioning,” in *Ground-based Instrumentation for Astronomy*, SPIE, Sep. 2004, p. 1510. doi: 10.1117/12.551286.

[11] E. D. González-Carretero *et al.*, “GRANCAIN: the first light infrared camera for the adaptive optics of GTC: optical and mechanical design status,” in *Advances in Optical and Mechanical Technologies for Telescopes and Instrumentation V*, R. Navarro and R. Geyl, Eds., SPIE, 2022, p. 121881Q. doi: 10.1117/12.2627957.

[12] “National Instituto of Standards and Technologies.” Accessed: Jul. 12, 2024. [Online]. Available: https://trc.nist.gov/cryogenics/materials/references.htm.